

Massively Multitask Networks for Drug Discovery

Bharath Ramsundar^{*,†,°}

Steven Kearnes^{*,†}

Patrick Riley[°]

Dale Webster[°]

David Konerding[°]

Vijay Pande[†]

(^{*}Equal contribution, [†]Stanford University, [°]Google Inc.)

RBHARATH@STANFORD.EDU

KEARNES@STANFORD.EDU

PFR@GOOGLE.COM

DRW@GOOGLE.COM

DEK@GOOGLE.COM

PANDE@STANFORD.EDU

Abstract

Massively multitask neural architectures provide a learning framework for drug discovery that synthesizes information from many distinct biological sources. To train these architectures at scale, we gather large amounts of data from public sources to create a dataset of nearly 40 million measurements across more than 200 biological targets. We investigate several aspects of the multitask framework by performing a series of empirical studies and obtain some interesting results: (1) massively multitask networks obtain predictive accuracies significantly better than single-task methods, (2) the predictive power of multitask networks improves as additional tasks and data are added, (3) the total amount of data and the total number of tasks both contribute significantly to multitask improvement, and (4) multitask networks afford limited transferability to tasks not in the training set. Our results underscore the need for greater data sharing and further algorithmic innovation to accelerate the drug discovery process.

1. Introduction

Discovering new treatments for human diseases is an immensely complicated challenge. Prospective drugs must attack the source of an illness, but must do so while satisfying restrictive metabolic and toxicity constraints. Traditionally, drug discovery is an extended process that takes years to move from start to finish, with high rates of failure along the way.

After a suitable target has been identified, the first step in the drug discovery process is “hit finding.” Given some druggable target, pharmaceutical companies will screen millions of drug-like compounds in an effort to find a few attractive molecules for further optimization. These screens are often automated via robots, but are expensive to perform. Virtual screening attempts to replace or augment the high-throughput screening process by the use of computational methods (Shoichet, 2004). Machine learning methods have frequently been applied to virtual screening by training supervised classifiers to predict interactions between targets and small molecules.

There are a variety of challenges that must be overcome to achieve effective virtual screening. Low hit rates in experimental screens (often only 1–2% of screened compounds are active against a given target) result in imbalanced datasets that require special handling for effective learning. For instance, care must be taken to guard against unrealistic divisions between active and inactive compounds (“artificial enrichment”) and against information leakage due to strong similarity between active compounds (“analog bias”) (Rohrer & Baumann, 2009). Furthermore, the paucity of experimental data means that overfitting is a perennial thorn.

The overall complexity of the virtual screening problem has limited the impact of machine learning in drug discovery. To achieve greater predictive power, learning algorithms must combine disparate sources of experimental data across multiple targets. Deep learning provides a flexible paradigm for synthesizing large amounts of data into predictive models. In particular, multitask networks facilitate information sharing across different experiments and compensate for the limited data associated with any particular experiment.

In this work, we investigate several aspects of the multitask learning paradigm as applied to virtual screening. We gather a large collection of datasets containing nearly 40

million experimental measurements for over 200 targets. We demonstrate that multitask networks trained on this collection achieve significant improvements over baseline machine learning methods. We show that adding more tasks and more data yields better performance. This effect diminishes as more data and tasks are added, but does not appear to plateau within our collection. Interestingly, we find that the total amount of data and the total number of tasks both have significant roles in this improvement. Furthermore, the features extracted by the multitask networks demonstrate some transferability to tasks not contained in the training set. Finally, we find that the presence of shared active compounds is moderately correlated with multitask improvement, but the biological class of the target is not.

2. Related Works

Machine learning has a rich history in drug discovery. Early work combined creative featurizations of molecules with off-the-shelf learning algorithms to predict drug activity (Varnek & Baskin, 2012). The state of the art has moved to more refined models, such as the influence relevance voting method that combines low-complexity neural networks and k-nearest neighbors (Swamidass et al., 2009), and Bayesian belief networks that repurpose textual information retrieval methods for virtual screening (Abdo et al., 2010). Other related work uses deep recursive neural networks to predict aqueous solubility by extracting features from the connectivity graphs of small molecules (Lusci et al., 2013).

Deep learning has made inroads into drug discovery in recent years, most notably in 2012 with the Merck Kaggle competition (Dahl, November 1, 2012). Teams were given pre-computed molecular descriptors for compounds with experimentally measured activity against 15 targets and were asked to predict the activity of molecules in a held-out test set. The winning team used ensemble models including multitask deep neural networks, Gaussian process regression, and dropout to improve the baseline test set R^2 by nearly 17%. The winners of this contest later released a technical report that discusses the use of multitask networks for virtual screening (Dahl et al., 2014). Additional work at Merck analyzed the choice of hyperparameters when training single- and multitask networks and showed improvement over random forest models (Ma et al., 2015). The Merck Kaggle result has been received with skepticism by some in the cheminformatics and drug discovery communities (Lowe, December 11, 2012, and associated comments). Two major concerns raised were that the sample size was too small (a good result across 15 systems may well have occurred by chance) and that any gains in predictive accuracy were too small to justify the increase in complexity.

While we were preparing this work, a workshop paper was released that also used massively multitask networks for virtual screening (Unterthiner et al.). That work curated a dataset of 1,280 biological targets with 2 million associated data points and trained a multitask network. Their network has more tasks than ours (1,280 vs. 259) but far fewer data points (2 million vs. nearly 40 million). The emphasis of our work is considerably different; while their report highlights the performance gains due to multitask networks, ours is focused on disentangling the underlying causes of these improvements. Another closely related work proposed the use of collaborative filtering for virtual screening and employed both multitask networks and kernel-based methods (Erhan et al., 2006). Their multitask networks, however, did not consistently outperform single-task models.

Within the greater context of deep learning, we draw upon various strands of recent thought. Prior work has used multitask deep networks in the contexts of language understanding (Collobert & Weston, 2008) and multi-language speech recognition (Deng et al., 2013). Our best-performing networks draw upon design patterns introduced by GoogLeNet (Szegedy et al., 2014), the winner of ILSVRC 2014.

3. Methods

3.1. Dataset Construction and Design

Models were trained on 259 datasets gathered from publicly available data. These datasets were divided into four groups: PCBA, MUV, DUD-E, and Tox21. The PCBA group contained 128 experiments in the PubChem BioAssay database (Wang et al., 2012). The MUV group contained 17 challenging datasets specifically designed to avoid common pitfalls in virtual screening (Rohrer & Baumann, 2009). The DUD-E group contained 102 datasets that were designed for the evaluation of methods to predict interactions between proteins and small molecules (Mysinger et al., 2012). The Tox21 datasets were used in the recent Tox21 Data Challenge (<https://tripod.nih.gov/tox21/challenge/>) and contained experimental data for 12 targets relevant to drug toxicity prediction. We used only the training data from this challenge because the test set had not been released when we constructed our collection. In total, our 259 datasets contained 37.8M experimental data points for 1.6M compounds. Details for the dataset groups are given in Table 1. See the Appendix for details on individual datasets and their biological target categorization.

It should be noted that we did not perform any preprocessing of our datasets, such as removing potential experimental artifacts. Such artifacts may be due by com-

Table 1. Details for dataset groups. Values for the number of data points per dataset and the percentage of active compounds are reported as means, with standard deviations in parenthesis.

Group	Datasets	Data Points / ea.	% Active
PCBA	128	282K (122K)	1.8 (3.8)
DUD-E	102	14K (11K)	1.6 (0.2)
MUV	17	15K (1)	0.2 (0)
Tox21	12	6K (500)	7.8 (4.7)

pounds whose physical properties cause interference with experimental measurements or allow for promiscuous interactions with many targets. A notable exception is the MUV group, which has been processed with consideration of these pathologies (Rohrer & Baumann, 2009).

3.2. Small Molecule Featurization

We used extended connectivity fingerprints (ECFP4) (Rogers & Hahn, 2010) generated by RDKit (Landrum) to featurize each molecule. The molecule is decomposed into a set of fragments—each centered at a non-hydrogen atom—where each fragment extends radially along bonds to neighboring atoms. Each fragment is assigned a unique identifier, and the collection of identifiers for a molecule is hashed into a fixed-length bit vector to construct the molecular “fingerprint”. ECFP4 and other fingerprints are commonly used in cheminformatics applications, especially to measure similarity between compounds (Willett et al., 1998). A number of molecules (especially in the Tox21 group) failed the featurization process and were not used in training our networks. See the Appendix for details.

3.3. Validation Scheme and Metrics

The traditional approach for model evaluation is to have fixed training, validation, and test sets. However, the imbalance present in our datasets means that performance varies widely depending on the particular training/test split. To compensate for this variability, we used stratified K -fold cross-validation; that is, each fold maintains the active/inactive proportion present in the unsplit data. For the remainder of the paper, we use $K = 5$.

Note that we did not choose an explicit validation set. Several datasets in our collection have very few actives (~ 30 each for the MUV group), and we feared that selecting a specific validation set would skew our results. As a consequence, we suspect that our choice of hyperparameters may be affected by information leakage across folds. However, our networks do not appear to be highly sensitive to hyperparameter choice (see Section 4.1), so we do not consider leakage to be a serious issue.

Following recommendations from the cheminformatics

community (Jain & Nicholls, 2008), we used metrics derived from the receiver operating characteristic (ROC) curve to evaluate model performance. Recall that the ROC curve for a binary classifier is the plot of true positive rate (TPR) vs. false positive rate (FPR) as the discrimination threshold is varied. For individual datasets, we are interested in the area under the ROC curve (AUC), which is a global measure of classification performance (note that AUC must lie in the range $[0, 1]$). More generally, for a collection of N datasets, we consider the mean and median K -fold-average AUC:

$$\text{Mean / Median} \left\{ \frac{1}{K} \sum_{k=1}^K \text{AUC}_k(D_n) \mid n = 1, \dots, N \right\},$$

where $\text{AUC}_k(D_n)$ is defined as the AUC of a classifier trained on folds $\{1, \dots, K\} \setminus k$ of dataset D_n and tested on fold k . For completeness, we include in the Appendix an alternative metric called “enrichment” that is widely used in the cheminformatics literature (Jain & Nicholls, 2008). We note that many other performance metrics exist in the literature; the lack of standard metrics makes it difficult to do direct comparisons with previous work.

3.4. Multitask Networks

A neural network is a nonlinear classifier that performs repeated linear and nonlinear transformations on its input. Let \mathbf{x}_i represent the input to the i -th layer of the network (where \mathbf{x}_0 is simply the feature vector). The transformation performed is

$$\mathbf{x}_{i+1} = \sigma(\mathbf{W}_i \mathbf{x}_i + \mathbf{b}_i)$$

where \mathbf{W}_i and \mathbf{b}_i are respectively the weight matrix and bias for the i -th layer, and σ is a nonlinearity (in our work, the rectified linear unit (Nair & Hinton, 2010)). After L such transformations, the final layer of the network \mathbf{x}_L is then fed to a simple linear classifier, such as the softmax, which predicts the probability that the input \mathbf{x}_0 has label j :

$$P(y = j | \mathbf{x}_0) = \frac{e^{(\mathbf{w}^j)^T \mathbf{x}_L}}{\sum_{m=1}^M e^{(\mathbf{w}^m)^T \mathbf{x}_L}},$$

where M is the number of possible labels (here $M = 2$) and $\mathbf{w}^1, \dots, \mathbf{w}^M$ are weight vectors. \mathbf{W}_i , \mathbf{b}_i , and \mathbf{w}^m are learned during training by the backpropagation algorithm (Rumelhart et al., 1988). A multitask network attaches N softmax classifiers, one for each task, to the final layer \mathbf{x}_L . (A “task” corresponds to the classifier associated with a particular dataset in our collection, although we often use “task” and “dataset” interchangeably. See Figure 1.)

4. Experimental Section

In this section, we seek to answer a number of questions about the performance, capabilities, and limitations of mas-

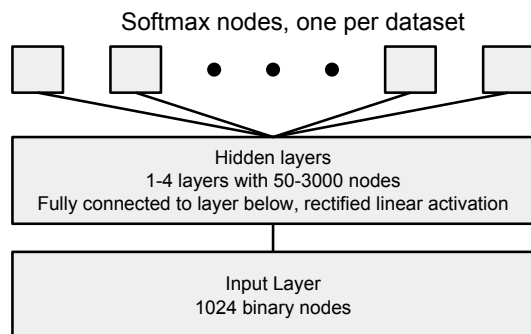


Figure 1. Multitask neural network.

sively multitask neural networks:

1. Do massively multitask networks provide a performance boost over simple machine learning methods? If so, what is the optimal architecture for massively multitask networks?
2. How does the performance of a multitask network depend on the number of tasks? How does the performance depend on the total amount of data?
3. Do massively multitask networks extract generalizable information about chemical space?
4. When do datasets benefit from multitask training?

The following subsections detail a series of experiments that seek to answer these questions.

4.1. Experimental Exploration of Massively Multitask Networks

We investigate the performance of multitask networks with various hyperparameters and compare to several standard machine learning approaches. Table 2 shows some of the highlights of our experiments. Our best multitask architecture (pyramidal multitask networks) significantly outperformed simpler models, including a hypothetical model whose performance on each dataset matches that of the best single-task model ($\text{Max}\{\text{LR}, \text{RF}, \text{STNN}, \text{PSTNN}\}$).

Every model we trained performed extremely well on the DUD-E datasets (all models in Table 2 had median 5-fold-average AUCs ≥ 0.99), making comparisons between models on DUD-E uninformative. For that reason, we exclude DUD-E from our subsequent statistical analysis. However, we did not remove DUD-E from the training altogether because doing so adversely affected performance on the other datasets (data not shown); we theorize that DUD-E helped to regularize the classifier and avoid overfitting.

During our first explorations, we had consistent problems

with the networks overfitting the data. As discussed in Section 3.1, our datasets had a very small fraction of positive examples. For the single hidden layer multitask network in Table 2, each dataset had 1200 associated parameters. With a total number of positives in the tens or hundreds, overfitting this number of parameters is a major issue in the absence of strong regularization.

Reducing the number of parameters specific to each dataset is the motivation for the pyramidal architecture. In our pyramidal networks, the first hidden layer is very wide (2000 nodes) with a second narrow hidden layer (100 nodes). This dimensionality reduction is similar in motivation and implementation to the 1x1 convolutions in the GoogLeNet architecture (Szegedy et al., 2014). The wide lower layer allows for complex, expressive features to be learned while the narrow layer limits the parameters specific to each task. Adding dropout of 0.25 to our pyramidal networks improved performance. We also trained single-task versions of our best pyramidal network to understand whether this design pattern works well with less data. Table 2 indicates that these models outperform vanilla single-task networks but do not substitute for multitask training. Results for a variety of alternate models are presented in the Appendix.

We investigated the sensitivity of our results to the sizes of the pyramidal layers by running networks with all combinations of hidden layer sizes: (1000, 2000, 3000) and (50, 100, 150). Across the architectures, means and medians shifted by $\leq .01$ AUC with only MUV showing larger changes with a range of .038. We note that performance is sensitive to the choice of learning rate and the number of training steps. See the Appendix for details and data.

4.2. Relationship between performance and number of tasks

The previous section demonstrated that massively multitask networks improve performance over single-task models. In this section, we seek to understand how multitask performance is affected by increasing the number of tasks. *A priori*, there are three reasonable “growth curves” (visually represented in Figure 2):

Over the hill: performance initially improves, hits a maximum, then falls.

Plateau: performance initially improves, then plateaus.

Still climbing: performance improves throughout, but with a diminishing rate of return.

We constructed and trained a series of multitask networks on datasets containing 10, 20, 40, 80, 160, and 249 tasks. These datasets all contain a fixed set of ten “held-in” tasks, which consists of a randomly sampled collection of five

Table 2. Median 5-fold-average AUCs for various models. For each model, the sign test in the last column estimates the fraction of datasets (excluding the DUD-E group, for reasons discussed in the text) for which that model is superior to the PMTNN (bottom row). We use the Wilson score interval to derive a 95% confidence interval for this fraction. Non-neural network methods were trained using scikit-learn (Pedregosa et al., 2011) implementations and basic hyperparameter optimization. We also include results for a hypothetical “best” single-task model ($\text{Max}\{\text{LR}, \text{RF}, \text{STNN}, \text{PSTNN}\}$) to provide a stronger baseline. Details for our cross-validation and training procedures are given in the Appendix.

Model	PCBA ($n = 128$)	MUV ($n = 17$)	Tox21 ($n = 12$)	Sign Test CI
Logistic Regression (LR)	.801	.752	.738	[.04, .13]
Random Forest (RF)	.800	.774	.790	[.06, .16]
Single-Task Neural Net (STNN)	.795	.732	.714	[.04, .12]
Pyramidal (2000, 100) STNN (PSTNN)	.809	.745	.740	[.06, .16]
$\text{Max}\{\text{LR}, \text{RF}, \text{STNN}, \text{PSTNN}\}$.824	.781	.790	[.12, .24]
1-Hidden (1200) Layer Multitask Neural Net (MTNN)	.842	.797	.785	[.08, .18]
Pyramidal (2000, 100) Multitask Neural Net (PMTNN)	.873	.841	.818	

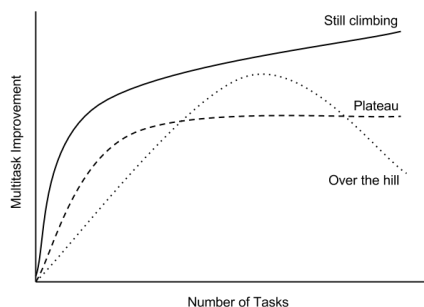


Figure 2. Potential multitask growth curves

PCBA, three MUV, and two Tox21 datasets. These datasets correspond to unique targets that do not have any obvious analogs in the remaining collection. (We also excluded a similarly chosen set of ten “held-out” tasks for use in Section 4.4). Each training collection is a superset of the preceding collection, with tasks added randomly. For each network in the series, we computed the mean 5-fold-average-AUC for the tasks in the held-in collection. We repeated this experiment ten times with different choices of random seed.

Figure 3 plots the results of our experiments. The shaded region emphasizes the average growth curve, while black dots indicate average results for different experimental runs. The figure also displays lines associated with each held-in dataset. Note that several datasets show initial dips in performance. However, all datasets show subsequent improvement, and all but one achieves performance superior to the single-task baseline. Within the limits of our current dataset collection, the distribution in Figure 3 agrees with either plateau or still climbing. The mean performance on the held-in set is still increasing at 249 tasks, so we hypoth-

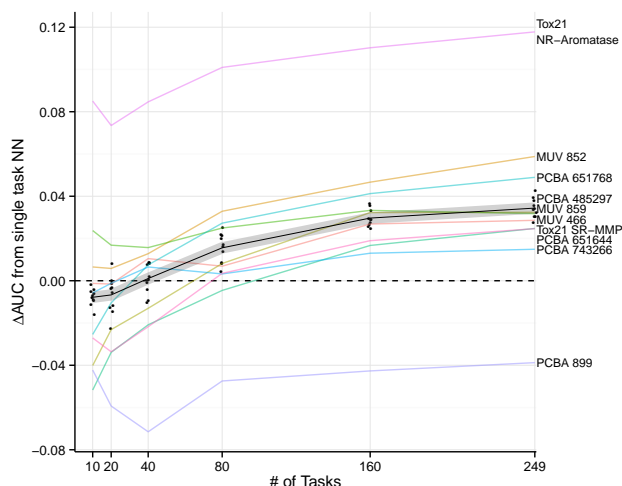


Figure 3. Held-in growth curves. The y -axis shows the change in AUC compared to a single-task neural network with the same architecture (PSTNN). Each colored curve is the multitask improvement for a given held-in dataset. Black dots represent means across the 10 held-in datasets for each experimental run, where additional tasks were randomly selected. The shaded curve is the mean across the 100 combinations of datasets and experimental runs.

esize that performance is **still climbing**. It is possible that our collection is too small and that an alternate pattern may eventually emerge.

4.3. More tasks or more data?

In the previous section we studied the effects of adding more tasks, but here we investigate the relative importance of the total amount of data vs. the total number of tasks. Namely, is it better to have many tasks with a small amount of associated data, or a small number of tasks with a large amount of associated data?

We constructed a series of multitask networks with 10, 15, 20, 30, 50 and 82 tasks. As in the previous section, the tasks are randomly associated with the networks in a cumulative manner (*i.e.*, the 82-task network contained all tasks present in the 50-task network, and so on). All networks contained the ten held-in tasks described in the previous section. The 82 tasks chosen were associated with the largest datasets in our collection, each containing 300K-500K data points. Note that all of these tasks belonged to the PCBA group.

We then trained this series of networks multiple times with 1.6M, 3.3M, 6.5M, 13M, and 23M data points sampled from the non-held-in tasks. We perform the sampling such that for a given task, all data points present in the first stage (1.6M) appeared in the second (3.3M), all data points present in the second stage appeared in the third (6.5M), and so on. We decided to use larger datasets so we could sample meaningfully across this entire range. Some combinations of tasks and data points were not realized; for instance, we did not have enough data to train a 20-task network with 23M additional data points. We repeated this experiment ten times using different random seeds.

Figure 4 shows the results of our experiments. The x -axis tracks the number of additional tasks, while the y -axis displays the improvement in performance for the held-in set relative to a multitask network trained only on the held-in data. When the total amount of data is fixed, having more tasks consistently yields improvement. Similarly, when the number of tasks is fixed, adding additional data consistently improves performance. Our results suggest that the total amount of data and the total number of tasks both contribute significantly to the multitask effect.

4.4. Do massively multitask networks extract generalizable features?

The features extracted by the top layer of the network represent information useful to many tasks. Consequently, we sought to determine the transferability of these features to tasks not in the training set. We held out ten data sets from the growth curves calculated in Section 4.2 and used the learned weights from points along the growth curves to initialize single-task networks for the held-out datasets, which we then fine-tuned.

The results of training these networks (with 5-fold stratified cross-validation) are shown in Figure 5. First, note that many of the datasets performed worse than the baseline when initialized from the 10-held-in-task networks. Further, some datasets never exhibited any positive effect due to multitask initialization. Transfer learning can be negative.

Second, note that the transfer learning effect became

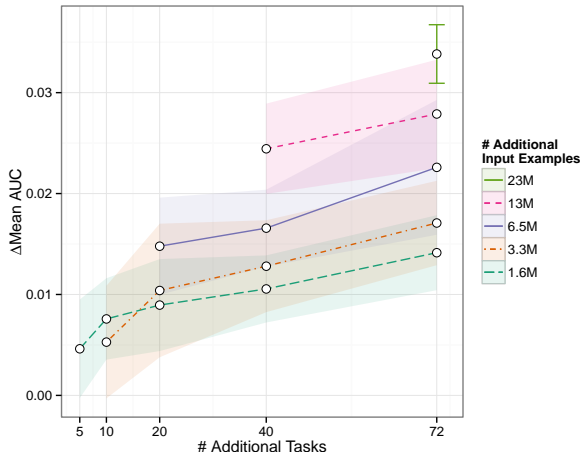


Figure 4. Multitask benefit from increasing tasks and data independently. As in Figure 2, we added randomly selected tasks (x -axis) to a fixed held-in set. A stratified random sampling scheme was applied to the additional tasks in order to achieve fixed total numbers of additional input examples (color, line type). White points indicate the mean over 10 experimental runs of Δ mean-AUC over the initial network trained on the 10 held-in datasets. Color-filled areas and error bars describe the smoothed 95% confidence intervals.

stronger as multitask networks were trained on more data. Large multitask networks exhibited better transferability, but the average effect even with 249 datasets was only $\sim .01$ AUC. We hypothesize that the extent of this generalizability is determined by the presence or absence of relevant data in the multitask training set.

4.5. When do datasets benefit from multitask training?

The results in Sections 4.2 and 4.4 indicate that some datasets benefit more from multitask training than others. In an effort to explain these differences, we consider three specific questions:

1. Do shared active compounds explain multitask improvement?
2. Do some biological target classes realize greater multitask improvement than others?
3. Do tasks associated with duplicated targets have artificially high multitask performance?

4.5.1. SHARED ACTIVE COMPOUNDS

The biological context of our datasets implies that active compounds contain more information than inactive compounds; while an inactive compound may be inactive for many reasons, active compounds often rely on similar physical mechanisms. Hence, shared active compounds should be a good measure of dataset similarity.

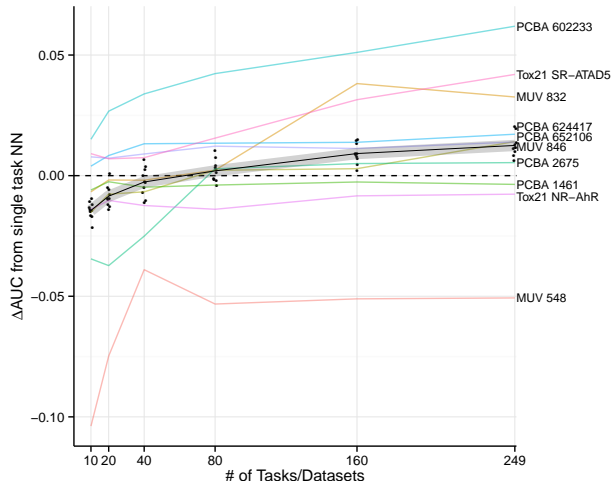


Figure 5. Held-out growth curves. The y -axis shows the change in AUC compared to a single-task neural network with the same architecture (PSTNN). Each colored curve is the result of initializing a single-task neural network from the weights of the networks from Section 4.2 and computing the mean across the 10 experimental runs. These datasets were *not* included in the training of the original networks. The shaded curve is the mean across the 100 combinations of datasets and experimental runs, and black dots represent means across the 10 held-out datasets for each experimental run, where additional tasks were randomly selected.

Figure 6 plots multitask improvement against a measure of dataset similarity we call “active occurrence rate” (AOR). For each active compound α in dataset D_i , $\text{AOR}_{i,\alpha}$ is defined as the number of additional datasets in which this compound is also active:

$$\text{AOR}_{i,\alpha} = \sum_{d \neq i} \mathbb{I}(\alpha \in \text{Actives}(D_d)).$$

Each point in Figure 6 corresponds to a single dataset D_i . The x -coordinate is

$$\text{AOR}_i = \text{Mean}_{\alpha \in \text{Actives}(D_i)} (\text{AOR}_{i,\alpha}),$$

and the y -coordinate ($\Delta \log\text{-odds-mean-AUC}$) is

$$\text{logit} \left(\frac{1}{K} \sum_{k=1}^K \text{AUC}_k^{(M)}(D_i) \right) - \text{logit} \left(\frac{1}{K} \sum_{k=1}^K \text{AUC}_k^{(S)}(D_i) \right),$$

where $\text{AUC}_k^{(M)}(D_i)$ and $\text{AUC}_k^{(S)}(D_i)$ are respectively the AUC values for the k -th fold of dataset i in the multitask and single-task models, and $\text{logit}(p) = \log(p/(1-p))$. The use of log-odds reduces the effect of outliers and emphasizes changes in AUC when the baseline is high. Note that for reasons discussed in Section 4.1, DUD-E was excluded from this analysis.

There is a moderate correlation between AOR and $\Delta \log\text{-odds-mean-AUC}$ ($r^2 = .33$); we note that this correlation is not present when we use $\Delta \text{mean-AUC}$ as the y -coordinate ($r^2 = .09$). We hypothesize that some portion of the multitask effect is determined by shared active compounds. That is, a dataset is most likely to benefit from multitask training when it shares many active compounds with other datasets in the collection.

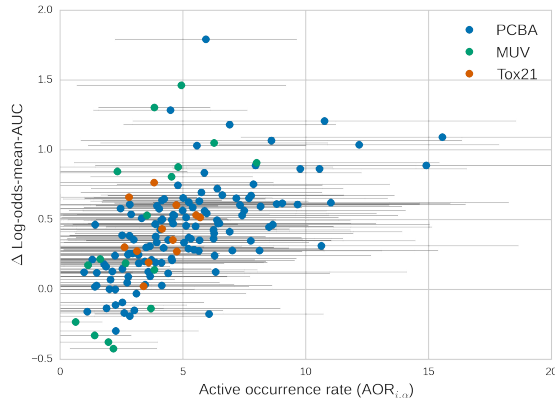


Figure 6. Multitask improvement compared to active occurrence rate (AOR). Each point in the figure represents a particular dataset D_i . The x -coordinate is the mean AOR across all active compounds in D_i , and the y -coordinate is the difference in log-odds-mean-AUC between multitask and single-task models. The gray bars indicate standard deviations around the AOR means. There is a moderate correlation ($r^2 = .33$). For reasons discussed in Section 4.1, we excluded DUD-E from this analysis. (Including DUD-E results in a similar correlation, $r^2 = .22$.)

4.5.2. TARGET CLASSES

Figure 7 shows the relationship between multitask improvement and target classes. As before, we report multitask improvement in terms of log-odds and exclude the DUD-E datasets. Qualitatively, no target class benefited more than any other from multitask training. Nearly every target class realized gains, suggesting that the multitask framework is applicable to experimental data from multiple target classes.

4.5.3. DUPLICATE TARGETS

As mentioned in Section 3.1, there are many cases of tasks with identical targets. We compared the multitask improvement of duplicate vs. unique tasks. The distributions have substantial overlap (see the Appendix), but the average log-odds improvement was slightly higher for duplicated tasks (.531 vs. .372; a one-sided t -test between the duplicate and unique distributions gave $p = .016$). Since duplicated targets are likely to share many active compounds, this improvement is consistent with the correlation seen in Sec-

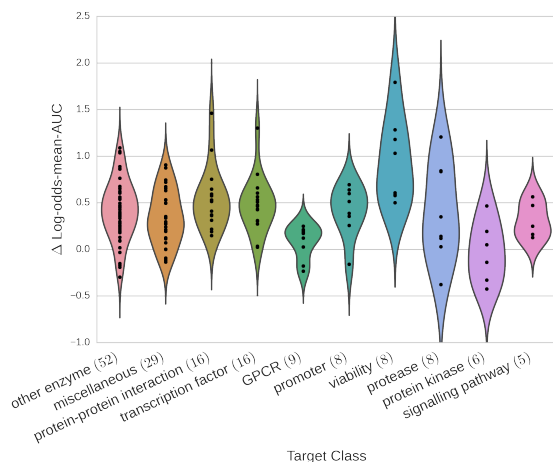


Figure 7. Multitask improvement across target classes. The x -coordinate lists a series of biological target classes represented in our dataset collection, and the y -coordinate is the difference in log-odds-mean-AUC between multitask and single-task models. Note that the DUD-E datasets are excluded. Classes are ordered by total number of targets (in parenthesis), and target classes with fewer than five members are merged into “miscellaneous.”

tion 4.5.1. However, sign tests for single-task vs. multitask models for duplicate and unique targets gave significant and highly overlapping confidence intervals ($[0.04, 0.24]$ and $[0.06, 0.17]$, respectively; recall that the meaning of these intervals is given in the caption for Table 2). Together, these results suggest that there is not significant information leakage within multitask networks. Consequently, the results of our analysis are unlikely to be significantly affected by the presence of duplicate targets in our dataset collection.

5. Discussion and Conclusion

In this work, we investigated the use of massively multitask networks for virtual screening. We gathered a large collection of publicly available experimental data that we used to train massively multitask neural networks. These networks achieved significant improvement over simple machine learning algorithms.

We explored several aspects of the multitask framework. First, we demonstrated that multitask performance improved with the addition of more tasks; our performance was still climbing at 259 tasks. Next, we considered the relative importance of introducing more data vs. more tasks. We found that additional data and additional tasks both contributed significantly to the multitask effect. We next discovered that multitask learning afforded limited transferability to tasks not contained in the training set. This effect was not universal, and required large amounts of data even when it did apply.

We observed that the multitask effect was stronger for some datasets than others. Consequently, we investigated possible explanations for this discrepancy and found that the presence of shared active compounds was moderately correlated with multitask improvement, but the biological class of the target was not. It is also possible that multitask improvement results from accurately modeling experimental artifacts rather than specific interactions between targets and small molecules. We do not believe this to be the case, as we demonstrated strong improvement on the thoroughly-cleaned MUV datasets.

The efficacy of multitask learning is directly related to the availability of relevant data. Hence, obtaining greater amounts of data is of critical importance for improving the state of the art. Major pharmaceutical companies possess vast private stores of experimental measurements; our work provides a strong argument that increased data sharing could result in benefits for all.

More data will maximize the benefits achievable using current architectures, but in order for algorithmic progress to occur, it must be possible to judge the performance of proposed models against previous work. It is disappointing to note that all published applications of deep learning to virtual screening (that we are aware of) use distinct datasets that are not directly comparable. It remains to future research to establish standard datasets and performance metrics for this field.

Another direction for future work is the further study of small molecule featurization. In this work, we use only one possible featurization (ECFP4), but there exist many others. Additional performance may also be realized by considering targets as well as small molecules in the featurization. Yet another line of research could improve performance by using unsupervised learning to explore much larger segments of chemical space.

Although deep learning offers interesting possibilities for virtual screening, the full drug discovery process remains immensely complicated. Can deep learning—coupled with large amounts of experimental data—trigger a revolution in this field? Considering the transformational effect that these methods have had on other fields, we are optimistic about the future.

Acknowledgments

B.R. was supported by the Fannie and John Hertz Foundation. S.K. was supported by a Smith Stanford Graduate Fellowship. We also acknowledge support from NIH and NSF, in particular NIH U54 GM072970 and NSF 0960306. The latter award was funded under the American Recovery and Reinvestment Act of 2009 (Public Law 111-5).

References

- Abdo, Ammar, Chen, Beining, Mueller, Christoph, Salim, Naomie, and Willett, Peter. Ligand-based virtual screening using bayesian networks. *Journal of chemical information and modeling*, 50(6):1012–1020, 2010.
- Collobert, Ronan and Weston, Jason. A unified architecture for natural language processing: Deep neural networks with multitask learning. In *Proceedings of the 25th international conference on Machine learning*, pp. 160–167. ACM, 2008.
- Dahl, George. Deep Learning How I Did It: Merck 1st place interview. *No Free Hunch*, November 1, 2012.
- Dahl, George E, Jaitly, Navdeep, and Salakhutdinov, Ruslan. Multi-task neural networks for QSAR predictions. *arXiv preprint arXiv:1406.1231*, 2014.
- Deng, Li, Hinton, Geoffrey, and Kingsbury, Brian. New types of deep neural network learning for speech recognition and related applications: An overview. In *Acoustics, Speech and Signal Processing (ICASSP), 2013 IEEE International Conference on*, pp. 8599–8603. IEEE, 2013.
- Erhan, Dumitru, L’Heureux, Pierre-Jean, Yue, Shi Yi, and Bengio, Yoshua. Collaborative filtering on a family of biological targets. *Journal of chemical information and modeling*, 46(2):626–635, 2006.
- Jain, Ajay N and Nicholls, Anthony. Recommendations for evaluation of computational methods. *Journal of computer-aided molecular design*, 22(3-4):133–139, 2008.
- Landrum, Greg. RDKit: Open-source cheminformatics. URL <http://www.rdkit.org>.
- Lowe, Derek. Did Kaggle Predict Drug Candidate Activities? Or Not? *In the Pipeline*, December 11, 2012.
- Lusci, Alessandro, Pollastri, Gianluca, and Baldi, Pierre. Deep architectures and deep learning in chemoinformatics: the prediction of aqueous solubility for drug-like molecules. *Journal of chemical information and modeling*, 53(7):1563–1575, 2013.
- Ma, Junshui, Sheridan, Robert P, Liaw, Andy, Dahl, George, and Svetnik, Vladimir. Deep neural nets as a method for quantitative structure-activity relationships. *Journal of Chemical Information and Modeling*, 2015.
- Mysinger, Michael M, Carchia, Michael, Irwin, John J, and Shoichet, Brian K. Directory of useful decoys, enhanced (DUD-E): better ligands and decoys for better benchmarking. *Journal of medicinal chemistry*, 55(14):6582–6594, 2012.
- Nair, Vinod and Hinton, Geoffrey E. Rectified linear units improve restricted boltzmann machines. In *Proceedings of the 27th International Conference on Machine Learning (ICML-10)*, pp. 807–814, 2010.
- Pedregosa, Fabian, Varoquaux, Gaël, Gramfort, Alexandre, Michel, Vincent, Thirion, Bertrand, Grisel, Olivier, Blondel, Mathieu, Prettenhofer, Peter, Weiss, Ron, Dubourg, Vincent, et al. Scikit-learn: Machine learning in python. *The Journal of Machine Learning Research*, 12:2825–2830, 2011.
- Rogers, David and Hahn, Mathew. Extended-connectivity fingerprints. *Journal of chemical information and modeling*, 50(5):742–754, 2010.
- Rohrer, Sebastian G and Baumann, Knut. Maximum unbiased validation (MUV) data sets for virtual screening based on pubchem bioactivity data. *Journal of chemical information and modeling*, 49(2):169–184, 2009.
- Rumelhart, David E, Hinton, Geoffrey E, and Williams, Ronald J. Learning representations by back-propagating errors. *Cognitive modeling*, 1988.
- Shoichet, Brian K. Virtual screening of chemical libraries. *Nature*, 432(7019):862–865, 2004.
- Swamidass, S Joshua, Azencott, Chloé-Agathe, Lin, Ting-Wan, Gramajo, Hugo, Tsai, Shiou-Chuan, and Baldi, Pierre. Influence relevance voting: an accurate and interpretable virtual high throughput screening method. *Journal of chemical information and modeling*, 49(4):756–766, 2009.
- Szegedy, Christian, Liu, Wei, Jia, Yangqing, Sermanet, Pierre, Reed, Scott, Anguelov, Dragomir, Erhan, Dumitru, Vanhoucke, Vincent, and Rabinovich, Andrew. Going deeper with convolutions. *arXiv preprint arXiv:1409.4842*, 2014.
- Unterthiner, Thomas, Mayr, Andreas, Unter Klambauer, G, Steijaert, Marvin, Wenger, Jörg, Ceulemans, Hugo, and Hochreiter, Sepp. Deep learning as an opportunity in virtual screening.
- Varnek, Alexandre and Baskin, Igor. Machine learning methods for property prediction in chemoinformatics: quo vadis? *Journal of chemical information and modeling*, 52(6):1413–1437, 2012.
- Wang, Yanli, Xiao, Jewen, Suzek, Tugba O, Zhang, Jian, Wang, Jiyao, Zhou, Zhigang, Han, Lianyi, Karapetyan, Karen, Dracheva, Svetlana, Shoemaker, Benjamin A, et al. PubChem’s BioAssay database. *Nucleic acids research*, 40(D1):D400–D412, 2012.

Willett, Peter, Barnard, John M, and Downs, Geoffrey M.
Chemical similarity searching. *Journal of chemical information and computer sciences*, 38(6):983–996, 1998.

Massively Multitask Networks for Drug Discovery: Appendix

February 11, 2022

A. Dataset Construction and Design

The PCBA datasets are dose-response assays performed by the NCATS Chemical Genomics Center (NCGC) and downloaded from PubChem BioAssay using the following search limits: TotalSidCount from 10000, ActiveSidCount from 30, Chemical, Confirmatory, Dose-Response, Target: Single, NCGC. These limits correspond to the search query: (10000[TotalSidCount] : 1000000000[TotalSidCount]) AND (30[ActiveSidCount] : 1000000000[ActiveSidCount]) AND "small_molecule"[filt] AND "doseresponse"[filt] AND 1[TargetCount] AND "NCGC"[SourceName]. We note that the DUD-E datasets are especially susceptible to "artificial enrichment" (unrealistic divisions between active and inactive compounds) as an artifact of the dataset construction procedure. Each data point in our collection was associated with a binary label classifying it as either active or inactive.

A description of each of our 259 datasets is given in Table A1. These datasets cover a wide range of target classes and assay types, including both cell-based and in vitro experiments. Datasets with duplicated targets are marked with an asterisk (note that only the non-DUD-E duplicate target datasets were used in the analysis described in the text). For the PCBA datasets, compounds not labeled "Active" were considered inactive (including compounds marked "Inconclusive"). Due to missing data in PubChem BioAssay and/or featurization errors, some data points and compounds were not used for evaluation of our models; failure rates for each dataset group are shown in Table A.2. The Tox21 group suffered especially high failure rates, likely due to the relatively large number of metallic or otherwise abnormal compounds that are not supported by the RDKit package. The counts given in Table A1 do not include these missing data. A graphical breakdown of the datasets by target class is shown in Figure A.1. The datasets used for the held-in and held-out analyses are repeated in Table A.3 and Table A.4, respectively.

As an extension of our treatment of task similarity in the text, we generated the heatmap in Figure A.2 to show the pairwise intersection between all datasets in our collection. A few characteristics of our datasets are immediately apparent:

- The datasets in the DUD-E group have very little intersection with any other datasets.
- The PCBA and Tox21 datasets have substantial self-overlap. In contrast, the MUV datasets have relatively little self-overlap.
- The MUV datasets have substantial overlap with the datasets in the PCBA group.
- The Tox21 datasets have very small intersections with datasets in other groups.

Figure A.3 shows the Δ log-odds-mean-AUC for datasets with duplicate and unique targets.

Dataset	Actives	Inactives	Target Class	Target
pcba-aid411*	1562	69 734	other enzyme	luciferase
pcba-aid875	32	73 870	protein-protein interaction	brca1-bach1
pcba-aid881	589	106 656	other enzyme	15hLO-2
pcba-aid883	1214	8170	other enzyme	CYP2C9
pcba-aid884	3391	9676	other enzyme	CYP3A4
pcba-aid885	163	12 904	other enzyme	CYP3A4

Massively Multitask Networks for Drug Discovery

Dataset	Actives	Inactives	Target Class	Target
pcba-aid887	1024	72 140	other enzyme	15hLO-1
pcba-aid891	1548	7836	other enzyme	CYP2D6
pcba-aid899	1809	7575	other enzyme	CYP2C19
pcba-aid902*	1872	123 512	viability	H1299-p53A138V
pcba-aid903*	338	54 175	viability	H1299-neo
pcba-aid904*	528	53 981	viability	H1299-neo
pcba-aid912	445	68 506	miscellaneous	anthrax LF-PA internalization
pcba-aid914	218	10 619	transcription fac- tor	HIF-1
pcba-aid915	436	10 401	transcription fac- tor	HIF-1
pcba-aid924*	1146	122 867	viability	H1299-p53A138V
pcba-aid925	39	64 358	miscellaneous	EGFP-654
pcba-aid926	350	71 666	GPCR	TSHR
pcba-aid927*	61	59 108	protease	USP2a
pcba-aid938	1775	70 241	ion channel	CNG
pcba-aid995*	699	70 189	signalling path- way	ERK1/2 cascade
pcba-aid1030	15 963	200 920	other enzyme	ALDH1A1
pcba-aid1379*	562	198 500	other enzyme	luciferase
pcba-aid1452	177	151 634	other enzyme	12hLO
pcba-aid1454*	536	130 788	signalling path- way	ERK1/2 cascade
pcba-aid1457	722	204 859	other enzyme	IMPase
pcba-aid1458	5805	202 680	miscellaneous	SMN2
pcba-aid1460*	5662	261 757	protein-protein interaction	K18
pcba-aid1461	2305	218 561	GPCR	NPSR
pcba-aid1468*	1039	270 371	protein-protein interaction	K18
pcba-aid1469	169	276 098	protein-protein interaction	TRb-SRC2
pcba-aid1471	288	223 321	protein-protein interaction	huntingtin
pcba-aid1479	788	275 479	miscellaneous	TRb-SRC2
pcba-aid1631	892	262 774	other enzyme	hPK-M2
pcba-aid1634	154	263 512	other enzyme	hPK-M2
pcba-aid1688	2374	218 200	protein-protein interaction	HTTQ103
pcba-aid1721	1087	291 649	other enzyme	LmPK
pcba-aid2100*	1159	301 145	other enzyme	alpha-glucosidase
pcba-aid2101*	285	321 268	other enzyme	glucocerebrosidase
pcba-aid2147	3477	223 441	other enzyme	JMJD2E
pcba-aid2242*	715	198 459	other enzyme	alpha-glucosidase
pcba-aid2326	1069	268 500	miscellaneous	influenza A NS1
pcba-aid2451	2008	285 737	other enzyme	FBPA
pcba-aid2517	1136	344 762	other enzyme	APE1
pcba-aid2528	660	347 283	other enzyme	BLM
pcba-aid2546	10 550	293 509	transcription fac- tor	VP16
pcba-aid2549	1210	233 706	other enzyme	RECQ1

Massively Multitask Networks for Drug Discovery

Dataset	Actives	Inactives	Target Class	Target
pcba-aid2551	16 666	288 772	transcription fac- tor	ROR gamma
pcba-aid2662	110	293 953	miscellaneous	MLL-HOX-A
pcba-aid2675	99	279 333	miscellaneous	MBNL1-CUG
pcba-aid2676	1081	361 124	GPCR	RFXFP1
pcba-aid463254*	41	330 640	protease	USP2a
pcba-aid485281	254	341 253	miscellaneous	apoferritin
pcba-aid485290	942	343 503	other enzyme	TDP1
pcba-aid485294*	148	362 056	other enzyme	AmpC
pcba-aid485297	9126	311 481	promoter	Rab9
pcba-aid485313	7567	313 119	promoter	NPC1
pcba-aid485314	4491	329 974	other enzyme	DNA polymerase beta
pcba-aid485341*	1729	328 952	other enzyme	AmpC
pcba-aid485349	618	321 745	protein kinase	ATM
pcba-aid485353	603	328 042	protease	PLP
pcba-aid485360	1485	223 830	protein-protein interaction	L3MBTL1
pcba-aid485364	10 700	345 950	other enzyme	TGR
pcba-aid485367	557	330 124	other enzyme	PFK
pcba-aid492947	80	330 601	GPCR	beta2-AR
pcba-aid493208	342	43 647	protein kinase	mTOR
pcba-aid504327	759	380 820	other enzyme	GCN5L2
pcba-aid504332	30 586	317 753	other enzyme	G9a
pcba-aid504333	15 670	341 165	protein-protein interaction	BAZ2B
pcba-aid504339	16 857	367 661	protein-protein interaction	JMJD2A
pcba-aid504444	7390	353 475	transcription fac- tor	Nrf2
pcba-aid504466	4169	325 944	viability	HEK293T-ELG1-luc
pcba-aid504467	7647	322 464	promoter	ELG1
pcba-aid504706	201	321 230	miscellaneous	p53
pcba-aid504842	101	329 517	other enzyme	Mm-CPN
pcba-aid504845	104	385 400	miscellaneous	RGS4
pcba-aid504847	3515	390 525	transcription fac- tor	VDR
pcba-aid504891	34	383 652	other enzyme	Pin1
pcba-aid540276*	4494	279 673	miscellaneous	Marburg virus
pcba-aid540317	2126	381 226	protein-protein interaction	HP1-beta
pcba-aid588342*	25 034	335 826	other enzyme	luciferase
pcba-aid588453*	3921	382 731	other enzyme	TrxR1
pcba-aid588456*	51	386 206	other enzyme	TrxR1
pcba-aid588579	1987	393 298	other enzyme	DNA polymerase kappa
pcba-aid588590	3936	382 117	other enzyme	DNA polymerase iota
pcba-aid588591	4715	383 994	other enzyme	DNA polymerase eta
pcba-aid588795	1308	384 951	other enzyme	FEN1
pcba-aid588855	4894	398 438	transcription fac- tor	Smad3
pcba-aid602179	364	387 230	other enzyme	IDH1
pcba-aid602233	165	380 904	other enzyme	PGK

Massively Multitask Networks for Drug Discovery

Dataset	Actives	Inactives	Target Class	Target
pcba-aid602310	310	402 026	protein-protein interaction	Vif-A3G
pcba-aid602313	762	383 076	protein-protein interaction	Vif-A3F
pcba-aid602332	70	415 773	promoter	GRP78
pcba-aid624170	837	404 440	other enzyme	GLS
pcba-aid624171	1239	402 621	transcription factor	Nrf2
pcba-aid624173	488	406 224	other enzyme	PYK
pcba-aid624202	3968	372 045	promoter	BRCA1
pcba-aid624246	101	367 273	miscellaneous	ERG
pcba-aid624287	423	334 388	signalling pathway	Gsgsp
pcba-aid624288	1356	336 077	signalling pathway	Gsgsp
pcba-aid624291	222	345 619	promoter	a7
pcba-aid624296*	9841	333 378	miscellaneous	DNA re-replication
pcba-aid624297*	6214	336 050	miscellaneous	DNA re-replication
pcba-aid624417	6388	398 731	GPCR	GLP-1
pcba-aid651635	3784	387 779	promoter	ATXN
pcba-aid651644	748	361 115	miscellaneous	Vpr
pcba-aid651768	1677	362 320	other enzyme	WRN
pcba-aid651965	6422	331 953	protease	ClpP
pcba-aid652025	238	364 365	signalling pathway	IL-2
pcba-aid652104	7126	396 566	miscellaneous	TDP-43
pcba-aid652105	4072	324 774	other enzyme	PI5P4K
pcba-aid652106	496	368 281	miscellaneous	alpha-synuclein
pcba-aid686970	5949	358 501	viability	HT-1080-NT
pcba-aid686978*	62 746	354 086	viability	DT40-hTDP1
pcba-aid686979*	48 816	368 048	viability	DT40-hTDP1
pcba-aid720504	10 170	353 881	protein kinase	Plk1 PBD
pcba-aid720532*	945	14 532	miscellaneous	Marburg virus
pcba-aid720542	733	363 349	protein-protein interaction	AMA1-RON2
pcba-aid720551*	1265	342 387	ion channel	KCHN2 3.1
pcba-aid720553*	3260	338 810	ion channel	KCHN2 3.1
pcba-aid720579*	1913	304 815	miscellaneous	orthopoxvirus
pcba-aid720580*	1508	324 844	miscellaneous	orthopoxvirus
pcba-aid720707	268	364 332	other enzyme	EPAC1
pcba-aid720708	661	363 939	other enzyme	EPAC2
pcba-aid720709	516	364 084	other enzyme	EPAC1
pcba-aid720711	290	364 310	other enzyme	EPAC2
pcba-aid743255	902	388 656	protease	USP1/UAF1
pcba-aid743266	306	405 368	GPCR	PTHR1
muv-aid466	30	14 999	GPCR	S1P1 receptor
muv-aid548	30	15 000	protein kinase	PKA
muv-aid600	30	14 999	transcription factor	SF1
muv-aid644	30	14 998	protein kinase	Rho-Kinase2
muv-aid652	30	15 000	other enzyme	HIV RT-RNase
muv-aid689	30	14 999	other receptor	Eph rec. A4

Massively Multitask Networks for Drug Discovery

Dataset	Actives	Inactives	Target Class	Target
muv-aid692	30	15 000	transcription fac- tor	SF1
muv-aid712*	30	14 997	miscellaneous	HSP90
muv-aid713*	30	15 000	protein-protein interaction	ER-a-coact. bind.
muv-aid733	30	15 000	protein-protein interaction	ER-b-coact. bind.
muv-aid737*	30	14 999	protein-protein interaction	ER-a-coact. bind.
muv-aid810*	30	14 999	protein kinase	FAK
muv-aid832	30	15 000	protease	Cathepsin G
muv-aid846	30	15 000	protease	FXIa
muv-aid852	30	15 000	protease	FXIIa
muv-aid858	30	14 999	GPCR	D1 receptor
muv-aid859	30	15 000	GPCR	M1 receptor
tox-NR-AhR	768	5780	transcription fac- tor	Aryl hydrocarbon receptor
tox-NR-AR-LBD*	237	6520	transcription fac- tor	Androgen receptor
tox-NR-AR*	309	6955	transcription fac- tor	Androgen receptor
tox-NR-Aromatase	300	5521	other enzyme	Aromatase
tox-NR-ER-LBD*	350	6604	transcription fac- tor	Estrogen receptor alpha
tox-NR-ER*	793	5399	transcription fac- tor	Estrogen receptor alpha
tox-NR-PPAR-gamma*	186	6263	transcription fac- tor	PPAR γ
tox-SR-ARE	942	4889	miscellaneous	ARE
tox-SR-ATAD5	264	6807	promoter	ATAD5
tox-SR-HSE	372	6094	miscellaneous	HSE
tox-SR-MMP	919	4891	miscellaneous	mitochondrial membrane potential
tox-SR-p53	423	6351	miscellaneous	p53 signalling
dude-aa2ar	482	31 546	GPCR	Adenosine A2a receptor
dude-abl1	182	10 749	protein kinase	Tyrosine-protein kinase ABL
dude-ace	282	16 899	protease	Angiotensin-converting enzyme
dude-aces	453	26 240	other enzyme	Acetylcholinesterase
dude-ada	93	5450	other enzyme	Adenosine deaminase
dude-ada17	532	35 900	protease	ADAM17
dude-adrb1	247	15 848	GPCR	Beta-1 adrenergic receptor
dude-adrb2	231	14 997	GPCR	Beta-2 adrenergic receptor
dude-akt1	293	16 441	protein kinase	Serine/threonine-protein kinase AKT
dude-akt2	117	6899	protein kinase	Serine/threonine-protein kinase AKT2
dude-aldr	159	8999	other enzyme	Aldose reductase
dude-ampc	48	2850	other enzyme	Beta-lactamase
dude-andr*	269	14 350	transcription fac- tor	Androgen Receptor
dude-aofb	122	6900	other enzyme	Monoamine oxidase B
dude-bace1	283	18 097	protease	Beta-secretase 1

Massively Multitask Networks for Drug Discovery

Dataset	Actives	Inactives	Target Class	Target
dude-braf	152	9950	protein kinase	Serine/threonine-protein kinase B-raf
dude-cah2	492	31 168	other enzyme	Carbonic anhydrase II
dude-casp3	199	10 700	protease	Caspase-3
dude-cdk2	474	27 850	protein kinase	Cyclin-dependent kinase 2
dude-comt	41	3850	other enzyme	Catechol O-methyltransferase
dude-cp2c9	120	7449	other enzyme	Cytochrome P450 2C9
dude-cp3a4	170	11 800	other enzyme	Cytochrome P450 3A4
dude-csf1r	166	12 149	other receptor	Macrophage colony stimulating factor receptor
dude-cxcr4	40	3406	GPCR	C-X-C chemokine receptor type 4
dude-def	102	5700	other enzyme	Peptide deformylase
dude-dh11	330	19 350	other enzyme	11-beta-hydroxysteroid dehydrogenase 1
dude-dpp4	533	40 943	protease	Dipeptidyl peptidase IV
dude-drd3	480	34 037	GPCR	Dopamine D3 receptor
dude-dyr	231	17 192	other enzyme	Dihydrofolate reductase
dude-egfr	542	35 047	other receptor	Epidermal growth factor receptor erbB1
dude-esr1*	383	20 675	transcription factor	Estrogen receptor alpha
dude-esr2	367	20 190	transcription factor	Estrogen receptor beta
dude-fa10	537	28 315	protease	Coagulation factor X
dude-fa7	114	6250	protease	Coagulation factor VII
dude-fabp4	47	2750	miscellaneous	Fatty acid binding protein adipocyte
dude-fak1*	100	5350	protein kinase	FAK
dude-fgfr1	139	8697	other receptor	Fibroblast growth factor receptor 1
dude-fkbl1a	111	5800	other enzyme	FK506-binding protein 1A
dude-fnta	592	51 481	other enzyme	Protein farnesyltransferase/geranylgeranyltransferase type I alpha subunit
dude-fpps	85	8829	other enzyme	Farnesyl diphosphate synthase
dude-gcr	258	14 999	transcription factor	Glucocorticoid receptor
dude-glcm*	54	3800	other enzyme	glucocerebrosidase
dude-gria2	158	11 842	ion channel	Glutamate receptor ionotropic
dude-grik1	101	6549	ion channel	Glutamate receptor ionotropic kainate 1
dude-hdac2	185	10 299	other enzyme	Histone deacetylase 2
dude-hdac8	170	10 449	other enzyme	Histone deacetylase 8
dude-hivint	100	6650	other enzyme	Human immunodeficiency virus type 1 integrase
dude-hivpr	536	35 746	protease	Human immunodeficiency virus type 1 protease
dude-hivrt	338	18 891	other enzyme	Human immunodeficiency virus type 1 reverse transcriptase
dude-hmdh	170	8748	other enzyme	HMG-CoA reductase
dude-hs90a*	88	4849	miscellaneous	HSP90
dude-hxk4	92	4700	other enzyme	Hexokinase type IV

Massively Multitask Networks for Drug Discovery

Dataset	Actives	Inactives	Target Class	Target
dude-igflr	148	9298	other receptor	Insulin-like growth factor I receptor
dude-inha	43	2300	other enzyme	Enoyl-[acyl-carrier-protein] reductase
dude-ital	138	8498	miscellaneous	Leukocyte adhesion glycoprotein LFA-1 alpha
dude-jak2	107	6499	protein kinase	Tyrosine-protein kinase JAK2
dude-kif11	116	6849	miscellaneous	Kinesin-like protein 1
dude-kit	166	10 449	other receptor	Stem cell growth factor receptor
dude-kith	57	2849	other enzyme	Thymidine kinase
dude-kpcb	135	8700	protein kinase	Protein kinase C beta
dude-lck	420	27 397	protein kinase	Tyrosine-protein kinase LCK
dude-lkha4	171	9450	protease	Leukotriene A4 hydrolase
dude-mapk2	101	6150	protein kinase	MAP kinase-activated protein kinase 2
dude-mcr	94	5150	transcription factor	Mineralocorticoid receptor
dude-met	166	11 247	other receptor	Hepatocyte growth factor receptor
dude-mk01	79	4549	protein kinase	MAP kinase ERK2
dude-mk10	104	6600	protein kinase	c-Jun N-terminal kinase 3
dude-mk14	578	35 848	protein kinase	MAP kinase p38 alpha
dude-mmp13	572	37 195	protease	Matrix metalloproteinase 13
dude-mp2k1	121	8149	protein kinase	Dual specificity mitogen-activated protein kinase kinase 1
dude-nos1	100	8048	other enzyme	Nitric-oxide synthase
dude-nram	98	6199	other enzyme	Neuraminidase
dude-pa2ga	99	5150	other enzyme	Phospholipase A2 group IIA
dude-parp1	508	30 049	other enzyme	Poly [ADP-ribose] polymerase-1
dude-pde5a	398	27 547	other enzyme	Phosphodiesterase 5A
dude-pgh1	195	10 800	other enzyme	Cyclooxygenase-1
dude-pgh2	435	23 149	other enzyme	Cyclooxygenase-2
dude-plk1	107	6800	protein kinase	Serine/threonine-protein kinase PLK1
dude-pnph	103	6950	other enzyme	Purine nucleoside phosphorylase
dude-ppara	373	19 397	transcription factor	PPARa
dude-ppard	240	12 247	transcription factor	PPARd
dude-pparg*	484	25 296	transcription factor	PPARG
dude-prgr	293	15 648	transcription factor	Progesterone receptor
dude-ptn1	130	7250	other enzyme	Protein-tyrosine phosphatase 1B
dude-pur2	50	2698	other enzyme	GAR transformylase
dude-pygm	77	3948	other enzyme	Muscle glycogen phosphorylase
dude-pyrd	111	6450	other enzyme	Dihydroorotate dehydrogenase
dude-reni	104	6958	protease	Renin
dude-rock1	100	6299	protein kinase	Rho-associated protein kinase 1
dude-rxra	131	6948	transcription factor	Retinoid X receptor alpha
dude-sahh	63	3450	other enzyme	Adenosylhomocysteinase
dude-src	524	34 491	protein kinase	Tyrosine-protein kinase SRC

Massively Multitask Networks for Drug Discovery

Dataset	Actives	Inactives	Target Class	Target
dude-tgfr1	133	8500	other receptor	TGF-beta receptor type I
dude-thb	103	7448	transcription fac- tor	Thyroid hormone receptor beta-1
dude-thrb	461	26 999	protease	Thrombin
dude-try1	449	25 967	protease	Trypsin I
dude-tryb1	148	7648	protease	Tryptase beta-1
dude-tysy	109	6748	other enzyme	Thymidylate synthase
dude-urok	162	9850	protease	Urokinase-type plasminogen acti- vator
dude-vgfr2	409	24 946	other receptor	Vascular endothelial growth factor receptor 2
dude-wee1	102	6150	protein kinase	Serine/threonine-protein kinase WEE1
dude-xiap	100	5149	miscellaneous	Inhibitor of apoptosis protein 3

Table A.2. Featurization failures.

Group	Original	Featurized	Failure Rate (%)
PCBA	439 879	437 928	0.44
DUD-E	1 200 966	1 200 406	0.05
MUV	95 916	95 899	0.02
Tox21	11 764	7830	33.44

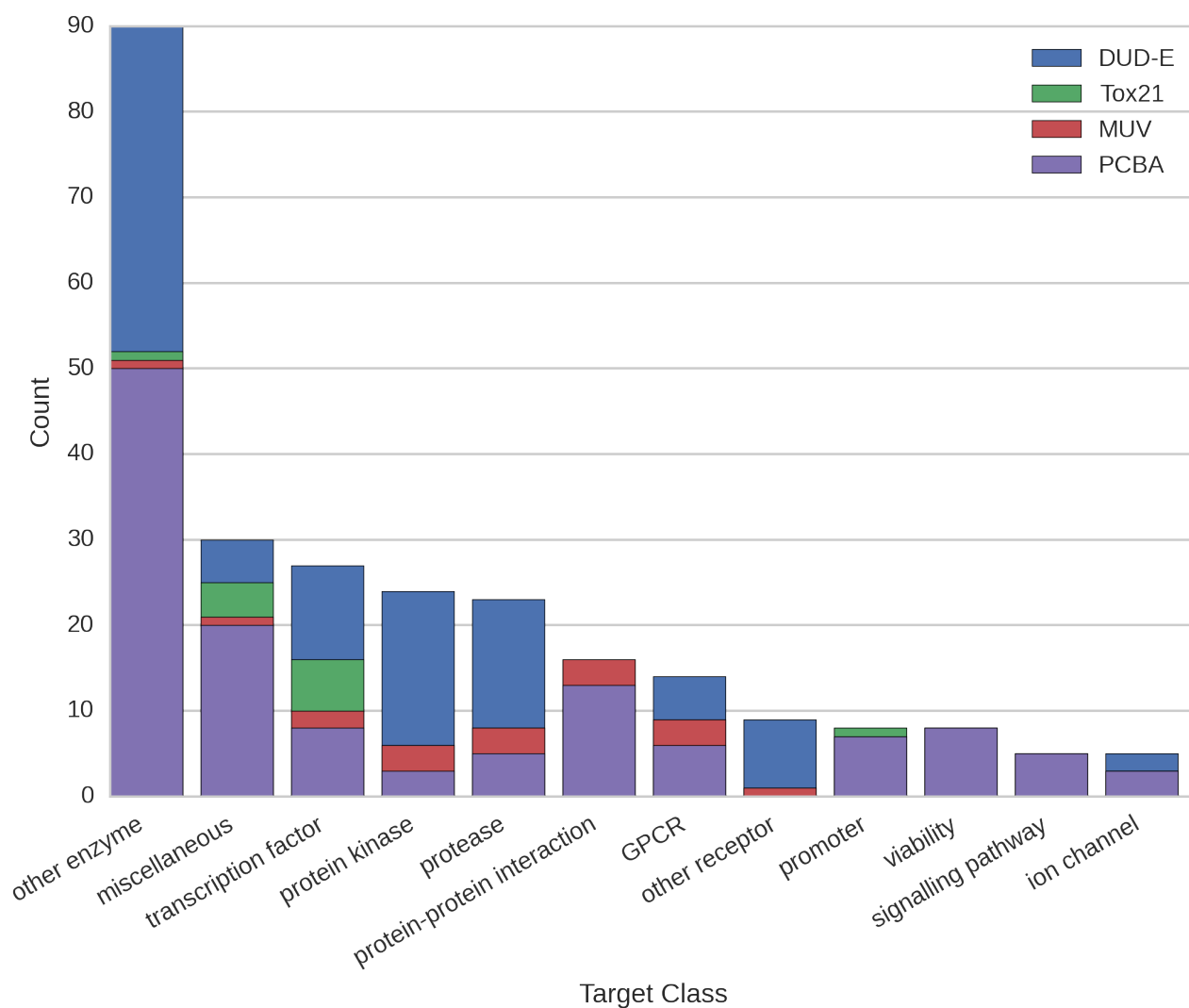


Figure A.1. Target class breakdown. Classes with fewer than five members were merged into the “miscellaneous” class.

Table A.3. Held-in datasets.

Dataset	Actives	Inactives	Target Class	Target
pcba-aid899	1809	7575	other enzyme	CYP2C19
pcba-aid485297	9126	311 481	promoter	Rab9
pcba-aid651644	748	361 115	miscellaneous	Vpr
pcba-aid651768	1677	362 320	other enzyme	WRN
pcba-aid743266	306	405 368	GPCR	PTHR1
muv-aid466	30	14 999	GPCR	S1P1 receptor
muv-aid852	30	15 000	protease	FXIIa
muv-aid859	30	15 000	GPCR	M1 receptor
tox-NR-Aromatase	300	5521	other enzyme	Aromatase
tox-SR-MMP	919	4891	miscellaneous	mitochondrial membrane potential

Table A.4. Held-out datasets.

Dataset	Actives	Inactives	Target Class	Target
pcba-aid1461	2305	218 561	GPCR	NPSR
pcba-aid2675	99	279 333	miscellaneous	MBNL1-CUG
pcba-aid602233	165	380 904	other enzyme	PGK
pcba-aid624417	6388	398 731	GPCR	GLP-1
pcba-aid652106	496	368 281	miscellaneous	alpha-synuclein
muv-aid548	30	15 000	protein kinase	PKA
muv-aid832	30	15 000	protease	Cathepsin G
muv-aid846	30	15 000	protease	FXIa
tox-NR-AhR	768	5780	transcription factor	Aryl hydrocarbon receptor
tox-SR-ATAD5	264	6807	promoter	ATAD5

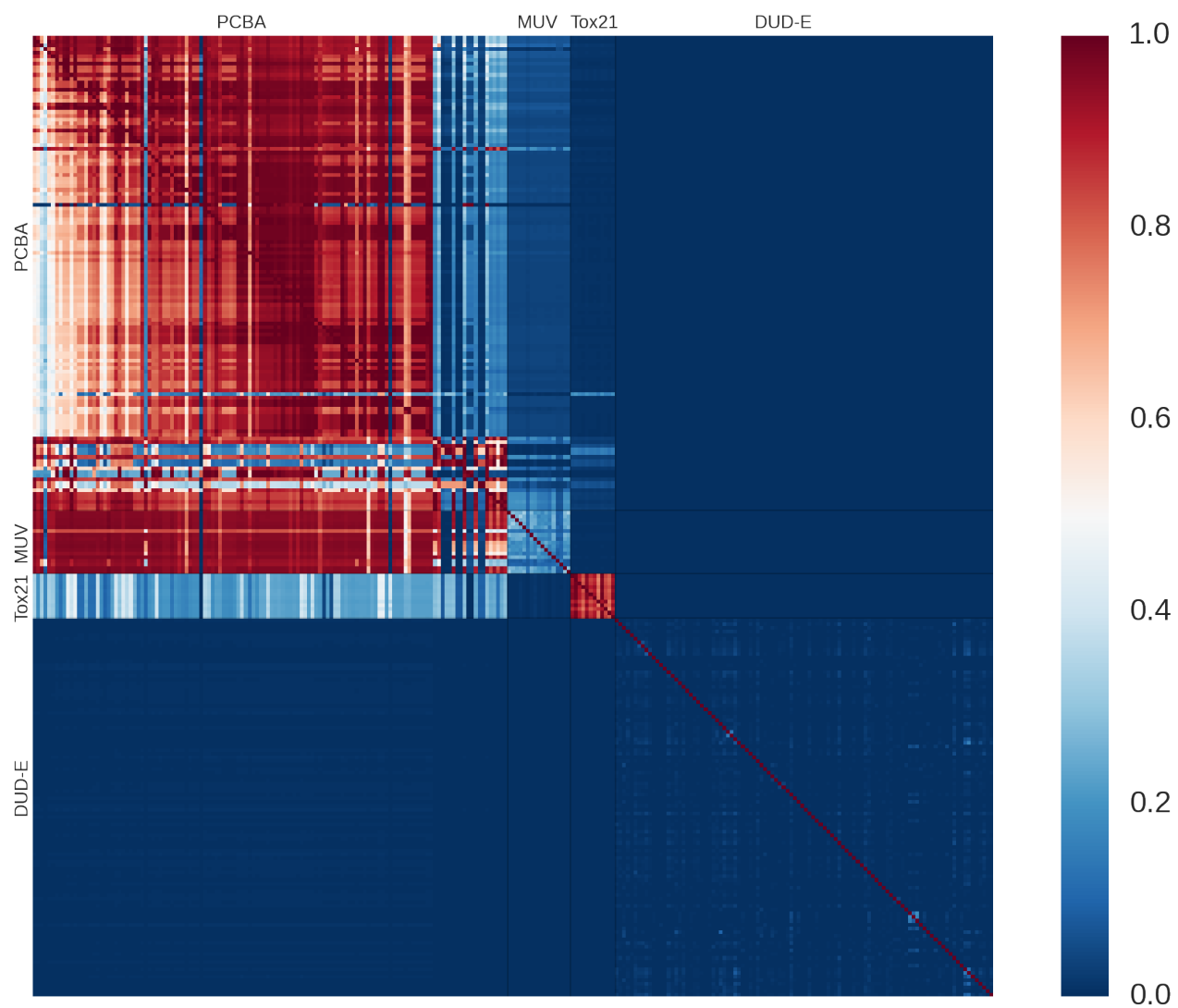


Figure A.2. Pairwise dataset intersections. The value of the element at position (x, y) corresponds to the fraction of dataset x that is contained in dataset y . Thin black lines are used to indicate divisions between dataset groups.

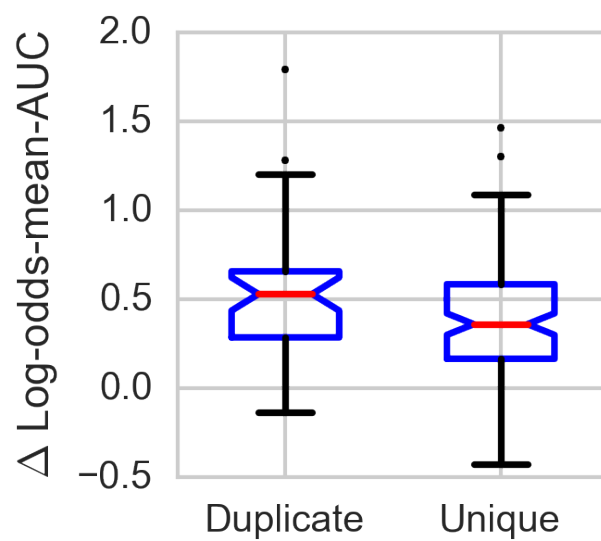


Figure A.3. Multitask performance of duplicate and unique targets. Outliers are omitted for clarity. Notches indicate a confidence interval around the median, computed as $\pm 1.57 \times \text{IQR} / \sqrt{N}$ (McGill et al., 1978).

B. Performance metrics

Table B.1. Sign test CIs for each group of datasets. Each model is compared to the Pyramidal (2000, 100) Multitask Neural Net, .25 Dropout model.

Model	PCBA ($n = 128$)	MUV ($n = 17$)	Tox21 ($n = 12$)
Logistic Regression (LR)	[.3, .11]	[.13, .53]	[.00, .24]
Random Forest (RF)	[.05, .16]	[.00, .18]	[.14, .61]
Single-Task Neural Net (STNN)	[.02, .10]	[.13, .53]	[.00, .24]
Pyramidal (2000, 100) STNN, .25 Dropout (PSTNN)	[.05, .15]	[.13, .53]	[.00, .24]
Max{LR, RF, STNN, PSTNN}	[.09, .21]	[.13, .53]	[.14, .61]
1-Hidden (1200) Layer Multitask Neural Net (MTNN)	[.05, .15]	[.22, .64]	[.01, .35]

Table B.2. Enrichment scores for all models reported in Table 2. Each value is the median across the datasets in a group of the mean k -fold enrichment values. Enrichment is an alternate measure of model performance common in virtual drug screening. We use the “ROC enrichment” definition from (Jain & Nicholls, 2008), but roughly enrichment is the factor better than random that a model’s top $X\%$ predictions are.

Model	PCBA				MUV				Tox21			
	0.5%	1%	2%	5%	0.5%	1%	2%	5%	0.5%	1%	2%	5%
LR	19.4	16.5	12.1	7.9	20.0	23.3	15.0	8.0	23.9	18.3	10.6	6.7
RF	40.0	27.4	17.4	9.1	40.0	26.7	16.7	7.3	23.2	19.5	13.6	7.8
STNN	19.0	15.6	11.8	7.7	26.7	20.0	11.7	8.0	16.2	14.4	9.8	6.1
PSTNN	21.8	16.9	12.4	7.9	26.7	16.7	13.3	8.0	23.8	16.1	10.0	6.7
MTNN	33.8	23.6	16.9	9.8	26.7	16.7	16.7	8.7	24.5	18.0	11.4	6.9
PMTNN	43.8	29.6	19.7	11.2	40.0	23.3	16.7	10.0	23.5	18.5	13.7	8.1

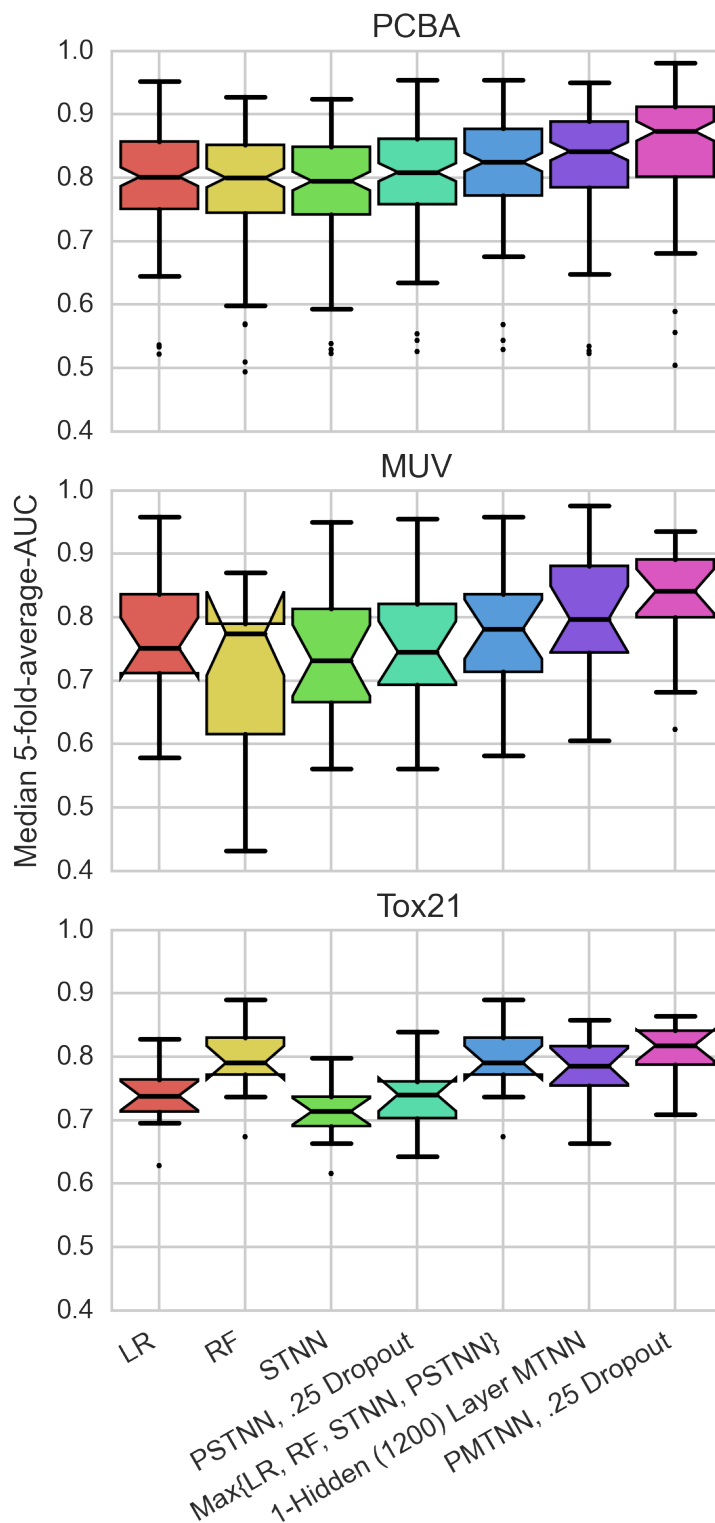


Figure B.1. Graphical representation of data from Table 2 in the text. Notches indicate a confidence interval around the median, computed as $\pm 1.57 \times \text{IQR} / \sqrt{N}$ (McGill et al., 1978). Occasionally the notch limits go beyond the quartile markers, producing a “folded down” effect on the boxplot. Paired t -tests (2-sided) relative to the PMTNN across all non-DUD-E datasets gave $p \leq 1.86 \times 10^{-15}$.

C. Training Details

The multitask networks in Table 2 were trained with learning rate .0003 and batch size 128 for 50M steps using stochastic gradient descent. Weights were initialized from a zero-mean Gaussian with standard deviation .01. The bias was initialized at .5. We experimented with higher learning rates, but found that the pyramidal networks sometimes failed to train (the top hidden layer zeroed itself out). However, this effect vanished with the lower learning rate. Most of the models were trained with 64 simultaneous replicas sharing their gradient updates, but in some cases we used as many as 256.

The pyramidal single-task networks were trained with the same settings, but for 100K steps. The vanilla single-task networks were trained with learning rate .001 for 100K steps. The networks used in Figure 3 and Figure 4 were trained with learning rate 0.003 for 500 epochs plus a constant 3 million steps. The constant factor was introduced after we observed that the smaller multitask networks required more epochs than the larger networks to stabilize.

The networks in Figure 5 were trained with a Pyramidal (1000, 50) Single Task architecture (matching the networks in Figure 3). The weights were initialized with the weights from the networks represented in Figure 3 and then trained for 100K steps with a learning rate of 0.0003.

As we noted in the main text, the datasets in our collection contained many more inactive than active compounds. To ensure the actives were given adequate importance during training, we weighted the actives for each dataset to have total weight equal to the number of inactives for that dataset (inactives were given unit weight).

Table C.1 contains the results of our pyramidal model sensitivity analysis. Tables C.2 and C.3 give results for a variety of additional models not reported in Table 2.

Table C.1. Pyramid sensitivity analysis. Median 5-fold-average-AUC values are given for several variations of the pyramidal architecture. In an attempt to avoid the problem of training failures due to the top layer becoming all zero early in the training, the learning rate was set to 0.0001 for the first 2M steps then to 0.0003 for 28M steps.

Model	PCBA ($n = 128$)	MUV ($n = 17$)	Tox21 ($n = 12$)
Pyramidal (1000, 50) MTNN	.846	.825	.799
Pyramidal (1000, 100) MTNN	.845	.818	.796
Pyramidal (1000, 150) MTNN	.842	.812	.798
Pyramidal (2000, 50) MTNN	.846	.819	.794
Pyramidal (2000, 100) MTNN	.846	.821	.798
Pyramidal (2000, 150) MTNN	.845	.839	.792
Pyramidal (3000, 50) MTNN	.848	.801	.796
Pyramidal (3000, 100) MTNN	.844	.804	.799
Pyramidal (3000, 150) MTNN	.843	.810	.789

Table C.2. Descriptions for additional models. MTNN: multitask neural net. “Auxiliary heads” refers to the attachment of independent softmax units for each task to hidden layers (see Szegedy et al., 2014). Unless otherwise marked, assume 10M training steps.

A	8-Hidden (300) Layer MTNN, auxiliary heads attached to hidden layers 3 and 6, 6M steps
B	1-Hidden (3000) Layer MTNN, 1M steps
C	1-Hidden (3000) Layer MTNN, 1.5M steps
D	Pyramidal (1800, 100), 2 deep, reconnected (original input concatenated to first pyramid output)
E	Pyramidal (1800, 100), 3 deep
F	4-Hidden (1000) Layer MTNN, auxiliary heads attached to hidden layer 2, 4.5M steps
G	Pyramidal (2000, 100) MTNN, 10% connected
H	Pyramidal (2000, 100) MTNN, 50% connected
I	Pyramidal (2000, 100) MTNN, .001 learning rate
J	Pyramidal (2000, 100) MTNN, 50M steps, .0003 learning rate
K	Pyramidal (2000, 100) MTNN, .25 Dropout (first layer only), 50M steps
L	Pyramidal (2000, 100) MTNN, .25 Dropout, .001 learning rate

Table C.3. Median 5-fold-average AUC values for additional models. Sign test confidence intervals and paired *t*-test (2-sided) *p*-values are relative to the PMTNN from Table 2 and were calculated across all non-DUD-E datasets.

Model	PCBA (<i>n</i> = 128)	MUV (<i>n</i> = 17)	Tox21 (<i>n</i> = 12)	Sign Test CI	Paired <i>t</i> -Test
A	.836	.793	.786	[.01, .06]	9.37×10^{-43}
B	.835	.855	.769	[.11, .22]	1.17×10^{-17}
C	.837	.851	.765	[.12, .24]	2.60×10^{-16}
D	.842	.842	.816	[.08, .18]	1.89×10^{-21}
E	.842	.808	.789	[.02, .08]	9.25×10^{-43}
F	.858	.836	.810	[.10, .22]	4.85×10^{-13}
G	.831	.795	.774	[.03, .11]	1.15×10^{-31}
H	.856	.827	.796	[.04, .13]	5.34×10^{-21}
I	.860	.862	.824	[.07, .17]	6.23×10^{-14}
J	.830	.810	.801	[.05, .14]	9.25×10^{-25}
K	.859	.843	.803	[.24, .38]	3.25×10^{-9}
L	.872	.837	.802	[.35, .50]	2.74×10^{-2}

References

- Jain, Ajay N and Nicholls, Anthony. Recommendations for evaluation of computational methods. *Journal of computer-aided molecular design*, 22(3-4):133–139, 2008.
- McGill, Robert, Tukey, John W, and Larsen, Wayne A. Variations of box plots. *The American Statistician*, 32(1):12–16, 1978.
- Szegedy, Christian, Liu, Wei, Jia, Yangqing, Sermanet, Pierre, Reed, Scott, Anguelov, Dragomir, Erhan, Dumitru, Vanhoucke, Vincent, and Rabinovich, Andrew. Going deeper with convolutions. *arXiv preprint arXiv:1409.4842*, 2014.